Crystal structure, Hirschfield surface analysis, thermal and DFT investigation accomplished with photoluminescence study of bis(N, N-diethylethylendiammonium)decabromodiantimoinate(III)

Rim Essalhi[a,b], Mohammed.S.M. Abdelbaky[b], Slim Elleuch[c] , FatmaZouari[a] , Santiago García-Granda[b]

[a]*University of Sfax, Faculty of Sciences, Material and Environment Science Laboratory B.P. N°1171, 3000 Sfax/Tunisia*

[b]*Department of physical and analytical chemistry, Oviedo University-CINN, 33006 Oviedo, Spain*

[C] *University of Sfax, Faculty of Sciences, Applied Physic Laboratory BP. 1171, 3000 Sfax, Tunisia*

Corresponding author e-mail address: Salhirim129@yahoo.fr

Abstract:

The hybrid compound $[C_6H_{18}N_2]_2Sb_2Br_{10}$ wassynthesized by slow evaporation at room temperature. X-ray single crystal diffraction, Infrared spectroscopy coupled with DFT calculation, optical absorption, photoluminescence and thermal analysis were used to characterize the centrosymmetric compound. Crystallization was obtained in the monoclinic system **$P2_1/c$** space group with cell parameters: a = 10.7309 (3) Å, b = 10.5842 (3) Å, c = 14.5551 (4) Å, β = 96.962 (3) ° and Z = 4. Results showed that the structure is built up from bioctahedral $[Sb_2Br_{10}]^{4-}$ dimers composed of two equivalent distorted octahedrons sharing one edge and N, N-diethylethylendiammoniumcations. The cohesion and stabilization between these entities is performed via N-H···Br hydrogen bonds. Crystal structure analysis was supported with the Hirshfeld surface (HS) and fingerprint plots to identify the significant intermolecular interactions in the crystal network.Furthermore, Thermal analysis of the title compound revealed no phase transition in the temperature range between 25 and 450°. The X-ray powder was in agreement with the X-ray structure. Scanning electronic microscopy (SEM) was also carried out. The theoretical calculations were conducted using the DFT approach with

the B3LYP/LanL2DZ basis set todepict the vibrational IR spectrum of the investigated compound in its ground state. A satisfactory agreement was found between the calculated and experimental results for the structural parameters and the vibrational properties. Moreover, Photoluminescence measurements showed a strong emission line at 3.64eV, the unaided-eye detectable blue luminescence emission came from the excitonic transition in the Sb_2Br_{10} anions.

Keywords: X-ray diffraction, Hirschfeld surfaces, DFT calculations, Thermal analysis, Photoluminescence

1. INTRODUCTION:

Recently, great attention has been devoted to the large family of alkyl ammonium halogenoantimonates (III) and halogenobismuthates(III) with different aliphatic and aromatic amines.Their interesting physical and chemical properties, including magnetic or ferroelectric transitions, (super)conductivity), electroluminescence and photoluminescence[1–10], in technological innovations.In previous research works, many systems involving Sb and Bi atoms were synthesized and characterized [11-29], exhibiting a general formula of AxMyXz (where X = Cl, Br or I; M = Sb(III) or Bi(III); and A is an organic cation).Moreover, it is known that elements of groups 14 and 15 as Sb(III) and Bi(III) ions, are characterized by their ns^2 electronic lone pair which can be more or less stereochemically active and play a crucial role in the distortion of the MX_6 octahedra [30]. Besides, the attractive properties displayed by these systems, some interest has been directed towards halogenoantimonate(III) compounds in combination with organic cations , in fact ,the latter leading to an extensive family of antimony halogen anions :$[SbX_{n+3}]^{n-}$,$[Sb_2X_{n+6}]^{n-}$,$[Sb_3X_{n+9}]^{n-}$,$[Sb_4X_{n+12}]^{n-}$,$[Sb_6X_{n+18}]^{n-}$. [31,32] .The different types of arrangement identified for the $[Sb_yX_{n+z}]^{n-}$ groupings are illustrated in the flowchart in Figure1.

In these materials, the anionic sub-lattice built up of MX_6 coordination polyhedra can be isolated (0D) or linked in face edge or corner sharing forming infinite chains (1D) or (2D) or (3D) networks [18,33]attached to the organic cations by hydrogen bonds. The presence of intermolecular hydrogen bonds in molecular packing is dedicated to the stability of the complex. In this work, we report the synthesis of a new organic halogeno-antimoinate material, bis(N,N-diethylethylendiammonium) decabromodiantimoinate(III), $(C_6H_{18}N_2)_2$ Sb_2Br_{10} and its structural characterization by X-ray diffraction (XRD) accompanied with an insight into HS analysis, spectroscopic measurements (Fourier Transform Infrared (FT-IR) Spectroscopy,optical and photoluminescence analyses), thermal calorimetry (DSC and ATG)

as well as DFT.Calculations based on correlation between experimental vibrational spectra and computed results were also discussed.

2. EXPERIMENTAL:

2.1. Synthesis of $(C_6H_{18}N_2)_2\ Sb_2Br_{10}$

$(C_6H_{18}N_2)_2\ Sb_2Br_{10}$ single crystals were prepared by dissolving in hydrobromic acid, HBr (12 M) solution, a stoichiometric mixture of antimony (III) oxide Sb_2O_3 and N, N-diethylendiamine in the presence of ethanol. The resulting aqueous solute ion was evaporated slowly at room temperature. After 1 month, yellow prism crystals appeared with suitable dimensions for single structural analysis.

2. 2. X-ray data collection

A suitable colorless crystal of good quality with the dimension of $0.24 \times 0.07 \times 0.05\ mm^3$ was carefully picked by using a polarizing microscope for the XRD experiments and mounted on a glass fiber using glue.

The single-crystal diffraction data were collectedon an Oxford Diffraction Xcalibur Ruby Gemini S four-circle diffractometer equipped with graphite monochromatic Mo Kα radiation (0.71073 Å) at 293(2) K. Lattice parameters were found from the setting angles of 11614 reflections in the range of $2.64 \leq \theta \leq 31.42°$ where 5354 reflections had independent intensity of $I > 2\sigma(I)$. However, the structural model was solved in the monoclinic space group $P2_{1/C}$ by direct methods, using SHELXS-86 [34]while full matrix least-squares refinement on F^2 was delivered by the SHELXL-97 computational program [35]that give positions of antimony and bromine atoms. The molecular graphics of the compound were created with DIAMOND 3.2 version [36]**.**

2.3. Powder X-ray diffraction

Powder XRD (PXRD) measurements were recorded on a Siemens D5000 powder diffractometer, using Cu Kα radiation (1.5418 Å) with a 2θ range of 5–50° at room temperature. The PXRD pattern of the compound was compared with the theoretical one (Fig.2) indicating that the product was successfully obtained as pure crystalline phase.

2. 4. Micrographs and X-ray microanalysis

Scanning electron microscope (SEM) and Energy-dispersive X-ray spectroscopy (EDXS) were recordedby using JEOL-6610LV scanning electron microscope operating at 30 kV coupled with an Oxford X-Max microanalysis system (EDX).

2.5. Spectroscopic Measurements

The IR spectrum was recorded in the range of 4000-400 cm^{-1} with a FT-IR Bruker Tensor-27 spectrometer using a sample depressed in KBr pellet. This measure served to depict the functional groups and the molecular formula of the crystal The pellet was prepared by mixing 5% of powder sample with 95% of KBr and compressing the whole into a disk. Moreover, the room temperature photoluminescence spectrum was recorded using a time resolved Edimbugh Instruments FLSP920 spectrofluorimeter with a Red-PMT detector and a Xenon bulb as an excitation source. A conventional UV–visabsorptionspectrometer (Shimadzu UV 3101)was used to issue the optical absorption spectra at room temperature.

2.6. Thermal characterization.

A Mettler-Toledo TGA/SDTA851eand a DSC822e were used for the thermal analysis in oxygendynamic atmosphere (50 mL/min) at a heating rate of 10 °C/min. In this case, ca. 10 mg of powder sample was thermally treated, and blank runs were performed. In TG tests, a Pfeiffer vacuumThermoStarTM GSD301T mass spectrometer was used todetermine the evacuated vapours.

2.7.Hirshfeld surfaces analysis:

Molecular HS calculation was performed using the CrystalExplorer 3.1 [37]program in order to illustrate the main differences between the intermolecular contacts in the crystal structure.The distance from HS to the nearest nucleus inside and outside the surfacewas marked by *di* and *de* respectively, whereas *dnorm* is a normalized contact distance, which is defined in terms of *di*, *de* and the van der Waals (vdW) radii of atoms: [38]

$$d_{norm} = \frac{d_i - r_i^{vdw}}{r_i^{vdw}} + \frac{d_e - r_e^{vdw}}{r_e^{vdw}}$$

The *d norm* takes a negative valuen when intermolecular contacts are shorter thanvdW radii,and positive when it is longer. A red-white-blue color scheme refers to the mapping of *dnorm* values onto the HS. If the atoms make intermolecular contacts closer than the sum of their vdW radii, these contacts were represented as red spots on the surface. Longer contacts were blue, while white was used for contacts around the sum of the vdW radii [39].

A 2D fingerprint plot combining *de* and *di*presents proportions of these interactions' intermolecular contacts [40]. The fingerprint plots can be decomposed to highlight particular atom pairs in close contacts [41].

2.8. Computational details

Density Functional Theory calculations were performed using the Gaussian 09W program package [42], with the B3LYP functional [43-45]. Fig.S2, billustrates the optimized geometry of the title compound model. Since the cluster must contain heavy atoms, we selected the LanL2DZ as a basis set [46]. This cluster model, extracted from single crystal X-Ray data, is built up from one $[Sb_2Br_{10}]^{4-}$ line sharing bioctaedra and two $(C_6H_{18}N_2)^{2+}$ organic cations. The optimized singlet ground state geometry was reached with the default convergence criteria without any constraint on the geometry [47]and checked with the lack of any imaginary frequency. A common empirical scaling factor of 0.961 [48] was used for the calculated vibrational normal modes. The theoretical UV-Visible absorption spectrum and the computed electronic transitions are obtained using TDDFT calculation at the same level of theory.

3. RESULT AND DISCUSSION:

3. 1. Structure description:

The experimental details of the structure determination for the studied compound are presentedin Table 1. Values corresponding to the atomic coordinates for anisotropic and isotropic thermal parameters of all the atoms in the last refinement cycle whose are in Tables S1 and S2. The title compound crystallizes in the centrosymmetric monoclinic space group$P2_{1/C}$ (NO.14) with the following unit cell dimension a=10.7309(3) Å; b= 10.5842 (3) Å; c=14.555 (4) Å; β = 96 .962 (3) ^{o}, V = 1640.95 (8) $Å^3$ and Z=4. The single crystal XRD of the new compound shows that the asymmetric unit is comprised of one N, N-diethylethylendiammoniumcation, and one half of a decabromodiantimoinate (III) dimer (Fig.S1).In the crystalthe anions generate an inversion center in order to form a $Sb_2Br_{10}^{4-}$ dimer constituted of two octahedra $SbBr_6^{3-}$ sharing one edge (Fig.S2). This arrangement type of anions is similar to the model found in [19]. The anionic sublatticeis built of distorted $SbBr_6^{3-}$octahedra sharing one edge and forming one-dimensional zigzag $([SbBr_5]_n)^{2n-}$ chains along the b axis as shown in (Fig.3) [49].

Both experimental and calculated bond lengths and angles for the organic and inorganic groups are shown in Table 2. We firstly assert the good agreement between experimental and calculated

structural parameters, which reflects that the chosen cluster model can be appropriate for further investigation. In fact, the mean relative error between experimental and calculated bond distance and angles, for the $[Sb_2Br_{10}]^{-4}$bioctaedra, are 3.56 % and 7.27 % and 2.20 % and 0.97 %, for the $(C_6H_{18}N_2)^{+2}$ cation, respectively. It is noted that the Sb-Br distances range between 2.601 (7) and 3.207 (8) Å, and are significantly shorter than the sum of vdW radii of Sb and Br (4.7 Å according to Pauling) [50]. The longest distance at 3.207(4)Å is attributed to the bond involving bridging bromine atoms (Br5) and the shortest one at 2.601(7)Å is due to bonds involving axial terminal bromine atoms opposite to the bridging bromine atoms (Br3 and Br2). These distances are similar of the compound $(4\text{-}BrC_5H_4NH)_2SbBr_5$[51] , Table 3 contains a comparative study of the bonding distances of the antimonite analogous synthesized compounds based on the literature. In addition to the bond length differences, the Br–Sb–Br bond angles range between 87.53(3)° and 92.29(4)° for cis and from 176.95(4)° to 178.98 (4)° for trans arrangements. This result reveals a slight distortion of the $[SbBr_5]^{2-}$ square pyramidal (Table 2).These values agree well with those previously observed by $[C_5N_2H_{16}]_2SbBr_5$[52]. The stereochemical activity of the Sb lone electron pair (opposite to the atom Br2) resulted in a primary deformation, correlated to the distortion of the $[SbBr_5]^{2-}$square-pyramidal from [53-54].Secondary deformations also occurred and are coupled with the hydrogen bond interactions [55].In addition, distorted square pyramidal geometry confirmed by the **τ5** parameter proposed by Addison and al. [56],τ5=0.21(τ5= (β-α)/60°), where β and α are the largest coordination angles and β >α.The C–N bond length varies from 1.487(8) to 1.502(7) Å, while the C–C bond length varies from 1.494(8) to 1.503(9) Å. These values are comparable with previously obtained results [57].

Moreover, relatively weak N–H···Br hydrogen bonds (with the shortest N…Br distance of the order of 3.291 Å) connect the organic cations to the anionic unit (Table 4, Fig.4a and 4b). They contribute to the distorted square-pyramidal coordination alterations between equivalent Sb–Br bond lengths and angles. Hydrogen bonds favor the elongation of the terminal Sb–Br bonds in these atoms.

3. 2. Thermal study

Differential Scanning Calorimetry (DSC) Analysis:

DSC results showed an endothermic peak followed by exothermic ones as illustrated in Fig. 5. The endothermic peak at 234°C is attributed to the melting point of $[C_6H_{18}N_2]_2Sb_2Br_{10}$ (this result is confirmed by a measure of this temperature by a Köfler heating Bank), whilst the exothermic peak at 293°C is assigned to the decomposition of the title compound. [58].

Thermogravimetric analysis (TGA):

The TG/DTG curve of the compound in the 25-600°C rangeis shown in fig.6.The curves indicate the relationship between temperature change and weight loss of the sample.The TGA curve shows that no weight losses between 25°C and 245°C and hence this compound is stable up to about 245°C. It exhibits one-weight loss, around 348°C. This weight loss, which is equal to 85.12% (calculated weight loss 85.34 %), associated with exothermic peak at 293°C on DSC curve, corresponds to degradation of the organic entity.

3.3. Morphological characterization:

The surface morphology and particle size of the title compound'N, N-diethylethylendiammoniumdecabromoodiantimoinate(III)' are given in (Fig.7a and 7b).As can be seen from this figure, the compound consists of an assembly of crystal fragments having uniform distribution and a flat surface, which indicates good crystal quality.

The Energy-dispersive X-ray spectroscopy (EDX) spectrum of the title compound revealed the presence of all non-hydrogen atoms(fig.7c), Table 5 shows the observed and calculated atoms : antimony, Bromine, Carbon and Nitrogen .

3.4. Hirshfeld Surface

The HS is a useful tool in the exploration of the packing modes and intermolecular contacts.It allows the visualization and exploration of intermolecular close contacts of a structure[59]. The Hirshfeld *dnorm* surface, shape index and curvedness of the $[C_6H_{18}N_2]_2\ Sb_2Br_{10}$ are shown in (Fig.8). The red spots on the top and bottom of the *dnorm* surface are assigned to the N–H···Br hydrogen bond which shows the closest intermolecular interactions in the compound. The small, flat segments delineated by the blue outline in the surface mapped with curvedness indicate the absence of π- π stacking interactions in the structure. In addition, it is clear from the HS that the crystal structure of the title compound does not exhibit any π- π stacking interaction since there is no evidence of the adjacent red and blue triangles on the shape index surface (fig.7b)[60].

The interactions of molecules in the asymmetric unit is revealed via the 2D fingerprint maps, quantified in Fig.9 as a range of 0.6-2.8 A˚ view with the *de* and *di* distance scales on the graph axes, to highlight particular atom pair close contacts. With such a decomposition, it is made possible to distinguish contributions from different interaction types. Globally, intermolecular interactions of H/Br, Br/H and H/H were the most present in the crystal packing (68.2% and 19.9% respectively), including four H···Br hydrogen bonds in the structure (Table 4, Fig.

4b).vdW forces are recognized to exert a high influence on the stabilization of the packing in the crystal structure. While other intercontacts contribute less to the Hirshfeld surfaces: Sb-Br/Br-Sb (7.9%), Br-Br (3.7%) and Sb-H /H-Sb (0.3%).

The contributions rates corresponding to a variety of contacts in the title crystal structure are illustrated in Fig.S3. This quantitative conclusion shows that the HBr interactions represent the important percentage of total surface. The Hirshfeld surfaces certainly allow a detailed scrutiny by displaying all the intermolecular interactions taking place in the crystal . Crystal engineering can in fact draw largely upon this methodology.

3.5. Vibrational Study:

In this section, we further investigate the molecular structure of the compound by recording their experimental and theoretical IR absorption spectra. In Fig 10a and 10b, we present a superposition of these spectra in the low and high wavenumbers regions, respectively. All assignments of the observed vibrational modes, presented in Table 4, are done with the aid of the visual inspection of the wavenumbers calculated by the GaussView05 software [61] and by comparison with reported bibliographic data done on similar compounds [62-64].

Vibrational analysis results, detailed in table 6, assert the well resolved observed IR bands which can be a great signature of the highly ordered molecular structure and on the purity of our compound. As shown in Fig.10b, the experimental spectrum shows a broad IR absorption band located between 2800 cm^{-1} and 3200 cm^{-1}. From the calculated wavenumbers, this broad band seems to be assigned to all asymmetric and symmetric stretching modes of the NH_3, CH_3, CH_2 and NH groups (see table 7). In the same context, the asymmetric and symmetric deformation modes of these groups are assigned to the IR peaks between 1400 cm^{-1} and 1600 cm^{-1}.

Moreover, the wagging and twisting vibrational modes of CH_2 groups are assigned to the bands observed in the 1200 cm^{-1} - 1400 cm^{-1} wavenumbers region while the IR bands observed at 1177 cm^{-1} and 1108 cm^{-1} correspond to the rocking mode of the NH_3 and CH_3 groups, respectively. The IR band observed at 974 cm^{-1} and 943 $cm^{-1}$are assigned to the rocking mode of CH_2 groups and the peaks observed at 785 cm^{-1} correspond to the deformation mode of the same group. Finally, the stretching vibrations of the CN and CC bonds in the organic skeleton are located between 1000 cm^{-1} and 1100 cm^{-1}, while their corresponding deformation modes are assigned to the remaining band under 900 cm^{-1}.

3.6. Optical Study:

UV– visible absorption and photoluminescence techniques were used to study the optical behavior of the material. Moreover, TDDFT theory calculation was carried out and the theoretical absorption spectrum and electronic transitions were provided. In Fig 11, we gathered the experimental and theoretical UV-Visible absorption spectra along with the excitation and emission spectra of the $[C_6H_{18}N_2]_2\ Sb_2Br_{10}$ recorded at room temperature. As can be seen, two absorption bands located at 262 nm (4.73 eV) and 355 nm (3.49 eV) are observed. Also, under irradiation with a 3.64 eV excitation line, a strong blue luminescence is exhibited by the sample and observed at room temperature with the naked eye at 430 nm (2.88 eV) [65-68]. Since the used organic cation do not exhibit any conjugated electrons and seems to be optically transparent in this wavelength range, we deduced that all the observed features come from mainly electronic transitions within the inorganic sublattice.

In effect, the observed luminescence is believed to originate from radiative excitonic recombinations occurring within the bromoantimoinate inorganic part anions, rather than the organic layers. The UV spectrum shows absorption features typical of antimonite based hybrid organic-inorganic materials, and the band at 355 nm is assumed to come from the lowest excitonic state as reported in literature [69-72]. To boost this assumption, the excitation spectrum recorded at 426 nm, exhibits a sharp peak at 340 nm (3.64 eV) typically characteristic of the well known Wannier type excitons observed in similar compounds based on $SbBr_6$ octahedrons [69,72]. On the other hand, the higher energy absorption band is attributed to interband transitions mainly related with some Metal-Centered (MC) transitions as deduced from previously reported works [73-75]. For the theoretical results, the generated absorption spectrum from the lowest five electronic transitions is relatively in good agreement with the experimental absorption spectrum. Those transitions arise between the three highest HOMO's and two lowest LUMO's. All characteristics of such transitions are provided in Table 7 and the relevant frontier orbital representations in Fig S4. The three transitions computed at 369.93, 354.9 and 319.86 nm (Fig. 11) are in the same range of the observed excitonic band at 355 nm. From their orbital representations, they correspond to charge redistribution within the $SbBr_6$ octahedrons. On the other hand, the high energetic band at 362 nm is dealing well with the transitions computed at 273.06 and 251.33 nm which defined as transitions from the HOMO-2 level to LUMO and LUMO+1 levels, respectively. With respect to the frontier orbital representations, we are able to attribute this band to a charge transfer from the Bromine atoms to the Antimony atoms within the inorganic sublattice. Here, we worthily note the conformity between the attributions based on experimental finding and those based on the calculated

electronic transitions. Moreover, as can be seen in Fig S4, the organic cation do not present any charge distribution in those state and then it don't contribute in the electronic transitions observed in this range. Moreover, the computed HOMO-LUMO difference, almost related to the Gap energy, is about 3.9 eV, and this agree well with our hypothesis for the observed bands attributions as excitonic and interband transitions.

For more simplicity, a simple model illustrated in the formation and recombination process of the exciton in $[C_6H_{18}N_2]$ Sb_2Br_{10} is shown in Scheme1. Under the excitation of 340 nm irradiation, an electron (-) is excited from the valence band (VB) composed by Sb (5s) +Br (4p) orbitals to the conduction band (CB) formed by the Sb (5p) orbital, leaving a hole (+) in the VB. The electron (-) and the hole (+) move freely in the CB and VB, forming an exciton. A blue emission at 430 nm (3.64eV) is attributed to the recombination of the electron and hole in the exciton. .

4. CONCLUSION

In the present paper, we have reported the synthesis, structural determination, photoluminescence and vibrational spectroscopy coupled with the theoretical calculations of a new organic–inorganic material with the formula $(C_6H_{18}N_2)_2Sb_2Br_{10}$. It crystallizes in monoclinic system with Centro-symmetricspace group$P2_{1/C}$. In the crystal structure of this material, the asymmetric unit built of dimeric $[Sb_2Br_{10}]$ which has the geometry of two octahedrons sharing one edge, in the presence of two N, N-diethylethylendiammoniumcations, wherein the crystal packing cohesion is ensured by N–H···Br hydrogen bonds, which is confirmed by Hirshfeld surface analysis. The PXRD fits with single-crystal pattern. On the other hand, According to IR spectroscopy recorded in the range of [400–4000], the structural and vibrational characterisitics of the material that were calculated by DFT/B3LYP/LanL2DZ method are in good correlation with the experimental results. Thermal analysis of the title compound showed that crystal structure is stable and it does not undergo any phase transition in the temperature range between 300 and 650 K.

Acknowledgements

We acknowledge the Financial support from the Ministry of Higher Education and Scientific Research of Tunisia and Spanish Ministerio de Economía y Competitividad(MAT2016-78155-C2-1-R) and Gobierno del PrincipadodeAsturias (GRUPIN-IDI/2018/170) are acknowledged.The authors are thankful to Pr. KamelMaaloul,translator and Academic English expert for proofreading and polishing the language of the manuscript.

REFERENCES

[1] David B. Mitzi ,Organic-Inorganic Perovskites Containing Trivalent Metal Halide Layers: The Templating Influence of the Organic Cation Layer , Inorg. Chem. 39 (2000) 6107-6113. https://doi.org/10.1021/ic000794i .

[2] R. Jakubas, L. Sobczyk, Phase transitions in alkylammonium halogenoantimonates and bismuthates ,J.Phase Transit 20(1990) 163-193.https://doi.org/10.1080/01411599008206873.

[3] G. C. Papavassiliou, G. A. Mousdis, I. B. Koutselas, Some new organic–inorganic hybrid semiconductors based on metal halide units: structural, optical and related properties, J. Adv. Mater. Opt. Electron. 9 (1999) 265-271.https://doi.org/10.1002/1099-0712(199911/12)9:6<265::AID-AMO390>3.0.CO;2-6 .

[4] B. Kulicka, T. Lis, V. Kinzhybalo, R. Jakubas, A. Piecha, Novel anionic water-containing inorganic fragment in $[4\text{-}NH_2PyH]_8[Bi_2Cl_{11}]$ $[Bi_2Cl_9(H_2O)_2]$: Structural characterization, thermal, dielectric and vibrational properties, Polyhedron 29 (2010) 2014-2022. https://doi.org/10.1016/j.poly.2010.03.017 .

[5] V.Y. Kotov, A.B. Ilyukhin, N.P. Simonenko, S.A. Kozyukhin, Synthesis, thermal stability, crystal structure and optical properties of 1,1′-(1,n-alkanediyl)bis(4-methylpyridinium) bromobismuthates, Polyhedron 137 (2017) 122–126. https://doi.org/10.1016/j.poly.2017.08.016.

[6] D. Fredj, C Ben Hassen, S. Elleuch, H. Feki, N.C. Boudjada, T. Mhiri, M. Boujelbene, Structural, vibrational and optical properties of a new organic–inorganic material: $(C_5H_8N_3)_2[BiCl_5]$,Mater. Res. Bull. 85(2017) 23–29, https://hal.archives-ouvertes.fr/hal-02002611.

[7] L.-M. Wu, X.-T Wu, L. Chen, Structural overview and structure–property relationships of iodoplumbate and iodobismuthate, Coord. Chem. Rev. 253 (2009) 2787. https://doi.org/10.1016/j.ccr.2009.08.003 .

[8] C. Hrizi , A. Samet , Y.Abid , S. Chaabouni , M. Fliyou , A. Koumina , Crystal structure, vibrational and optical properties of a new self-organized material containing iodide anions of bismuth(III), $[C_6H_4(NH_3)_2]_2Bi_2I_{10}4H_2O$, J. Mol. Struct. 992 (2011) 96–101. https://doi.org/10.1016/j.molstruc.2011.02.051.

[9] M.-W. Yuan, L-.H. Li, L. Chen, Syntheses, Structures, and Theoretical Studies of New Mercury Iodobismuthates: $(Et_4N)_4(Bi_4Hg_2I_{20})$ and $(n\text{Bu}_4N)_2(Bi_2HgI_{10})$ J.Z. Anorg. Allg. Chem. 635 (2009) 1645. https://doi.org/10.1002/zaac.200801401.

[10] N. Louvain, N. Mercier, F. Boucher, α- to β-(dmes)BiI_5(dmes = Dimethyl(2-ethylammonium)sulfonium Dication): Umbrella Reversal of Sulfonium in the Solid State and Short I···I Interchain Contacts-Crystal Structures, Optical Properties, and Theoretical Investigations of 1D Iodobismuthates. Inorganic Chemistry,J. Inorg. Chem. 48 (2009) 3. https://doi.org/10.1021/ic801900r .

[11] J. M. Ryan, Z. Xu, $[C_6H_5NH(CH_3)_2]_2Te_2I_{10}$: Secondary I•••I Bonds Build up a 3D Network. Inorganic Chemistry, J.Inorg. Chem. 43 (2004) 4106. https://doi.org/10.1002/chin.200436013.

[12] D. B. Mitzi, Organic-Inorganic Perovskites Containing Trivalent Metal Halide Layers: The Templating Influence of the Organic Cation Layer, J. Inorg. Chem. 39 (2000) 6107-6113. https://doi.org/10.1021/ic000794i .

[13] S. Chaabouni, A. Hadrich, F. Romain and A.B. Salah, Crystal structure, DSC and Raman studies in $CH_3C_6H_4NH(CH_3)_2 \cdot SbCl_4$, J. Solid State Sci. 5 (2003) 1041-1046. https://doi.org/10.1016/S1293-2558(03)00130-4 .

[14] Jakubas, R., Rok, M., Mencel, K., Bator, G., & Piecha-Bisiorek, A. ,Correlation between crystal structure and polar (ferroelectric) properties of haloantimonates(III) and halobismuthates(III) hybrids. Inorganic Chemistry Frontiers (2020). https://doi.org/10.1039/D0QI00265H .

[15] R. Jakubas, Z. Ciunik, G. Bator, Ferroelectric properties of $[4{-}NH_2C_5H_4NH][SbCl_4]$, J. Phys. Rev. B 67 (2003) 241031.https://doi.org/10.1103/PhysRevB.67.024103.

[16] R. Jakubas, L. Sobczyk, Phase transitions in alkylammonium halogenoantimonates and bismuthates, J. Phase Transit. 20 (1990) 163-193. https://doi.org/10.1080/01411599008206873.

[17] V. Varma, R. Bhattacharjee, H.N. Vasan, C.N.R. Rao, Infrared and Raman spectroscopic investigations of methylammonium haloantimonates(III), $[N(CH_3)_{4-n}H_n]_3\ Sb_2X_9$ (n = 0–3, X = Cl or Br), through their phase transitions, J.Spectrochim. Acta A 48 (1992) 1631. https://doi.org/10.1016/0584-8539(92)80237-Q .

[18] L. Sobczyk, R. Jakubas, J. Zaleski, Self-Assembly of Sb(III) and Bi(III) Halo-Coordinatetl -Octahedra in Salts of Organic Cations.Structure, Properties and Phase Transitions, Pol. J. Chem. 71 (1997) 265-300.https://scholar.google.com/citations?user=gNg7AI8AAAAJ&hl=en.

[19] H. Khili, N. Chaari, M. Fliyou, S. Chaabouni, Synthesis, Crystal Structure and Vibrational Properties of bis (N-benzylmethylammonium) Pentachlorobismuthate (III), J. Advances in Chem. 8 (2014) 1156. https://doi.org/10.24297/jac.v8i2.4038 .

[20] H. Khili, N. Chaari, M. Fliyou, A. Koumina, S. Chaabouni, Synthesis, crystal structure and vibrational properties of bis(4-benzyl pyridinium) pentachlorobismuthate(III), Polyhedron 36 (2012) 30-37.https://doi.org/10.1016/j.poly.2012.01.016 .

[21] A. Rhandour, A. Ouasri, P. Roussel, A. Mazzah, Crystal structure and vibrational studies of butylenediammonium pentachlorobismuthate (III) hydrate $[NH_3(CH_2)_4NH_3]BiCl_5{\cdot}H_2O$, J. Mol. Struct. 990 (2011) 95. https://doi.org/10.1016/j.molstruc.2011.01.022 .

[22] Adonin, S. A., Sokolov, M. N., & Fedin, V. P.Polynuclear halide complexes of Bi(III): From structural diversity to the new properties. Coordination Chemistry Reviews, 312 (2016) 1–21. https://doi.org/10.1016/j.ccr.2015.10.010 .

[23] M. Chanski, A. Białonska, R. Jakubas, A. Piecha-Bisiorek, Structural characterization and properties of bis (1,4-H2-1,2,4-triazolium) pentachlorobismuthate (III) and cocrystal of ammonium chloride with tris (1,4-H2-1,2,4-triazolium) hexachlorobismuthate (III), Polyhedron 71 (2014) 69-74. https://doi.org/10.1016/j.poly.2013.12.038 .

[24] M. Bujak, J. Zaleski, Structure of chloroantimonates(III) with an imidazolium cation: $(C_3H_5N_2)[SbCl_4]$ and $(C_3H_5N_2)_2[SbCl_5]$, J. Mol. Struct. 647 (2003) 121-128. https://doi.org/10.1016/S0022-2860(02)00509-4 .

[25] Z. Aloui, V. Ferretti, S. Abid, M. Rzaigui, F. Lefebvre, C. Ben Nasr, Synthesis, crystal structure and characterization of a new organic–inorganic hybrid material: $[C_6H_{16}N_2O]SbCl_5$, J. Mol. Struct.1087 (2015) 26-32. https://doi.org/10.1016/j.molstruc.2015.01.028 .

[26] I. Płowas, P. Szklarz, R. Jakubas, G. Bator, Structural, thermal and dielectric studies on the novel solution grown (4-dimethylaminopyridinium) chloroantimonate(III) and chlorobismuthate(III) crystals, Mater. Res. Bull 46 (2011) 1177- 1185. https://doi.org/10.1016/j.materresbull.2011.04.013 .

[27] A.S. Rao, U. Baruah, S.K. Das, Stabilization of $[BiCl_6]^{3-}$ and $[Bi_2Cl_{10}]^{4-}$ with various organic precursors as cations leading to inorganic–organic supramolecular adducts: Syntheses, crystal structures and properties of $[C_5H_7N_2]_3[BiCl_6]$, $[C_5H_7N_2][C_5H_8N_2]$ $[BiCl_6]$ and $[C_{10}H_{10}N_2]_2[Bi_2Cl_{10}]$, J. Inorg. Chim. Acta 372 (2011) 206-212. https://doi.org/10.1016/j.ica.2011.01.109 .

[28] B. Kulicka, R. Jakubas, B. Bednarska-Bolek, G. Bator and Z. Ciunik, Crystal structure and phase transitions in dipropylammonium hexachloroantimonate(V): $[N(C_3H_7)_2H_2][SbCl_6]$ J. Mol. Struct. 792–793 (2006) 151. https://doi.org/10.1016/j.molstruc.2005.10.058 .

[29] Z. Aloui,V. Ferretti, S. Abid, F. Lefebvre, M. Rzaigui, C. Ben Nasr, Synthesis, crystal structure and vibrational spectroscopic analysis of tetrakis(5-amino-1-H-1,2,4-triazol-4-ium)

decachlorodibismuthate(III):$[C_2H_5N_4]_4Bi_2Cl_{10}$, J. Mol. Struct.1097 (2015) 166. https://doi.org/10.1016/j.molstruc.2015.05.023 .

[30] W. Bi, N. Leblanc, N. Mercier, P. Auban-Senzier, C. Pasquier, Thermally Induced Bi(III) Lone Pair Stereoactivity: Ferroelectric Phase Transition and Semiconducting Properties of (MV)BiBr5 (MV= methylviologen), Chem. Mater. 21 (2009) 4099- 4101. https://doi.org/10.1021/cm9016003 .

[31]A. Ahmed, R. Blachnik, H. Reuter and H. Eickmeier ,J. Z. Kristallogr. 216 (2001) 207-208 , Crystal structure of tris(ethyldimethylphenylammonium) nonabromodiantimonate(III), $[EtMe_2PhN]_3[Sb_2Br_9]$. https://doi.org/10.1524/ncrs.2001.216.14.217.

[32] W. Medycki, K. Holderna-Natkaniec, J. Swiergiel, and R. Jakubas , Solid State Nucl. Magn. Reson. 24 (2003) 209–217 , Molecular dynamics in ferroelectric 4-aminopyridinium tetrachloroantimonate(III), $[4\text{-}NH_2C_5H_4NH][SbCl_4]$. http://www.elsevier.com/locate/ssnmr .

[33] S. A. Adonin, M. I. Rakhmanova, D. G. Samsonenko, M. N.Sokolov, V. P. Fedin, Hybrid salts of binuclear Bi(III) halide complexes with 1,2-bis(pyridinium)ethane cation: Synthesis, structure and luminescent behavior, Inorg. Chim. Acta 450 (2016) 232–235. http://dx.doi.org/10.1016/j.ica.2016.06.010 .

[34] G.M. Sheldrick, SHELXS-86, Program for Crystal Structure Solution, University of Göttingen, Germany (1986).

[35] G.M. Sheldrick, SHELXL-97, Program for Refinement of Crystal Structures ,University of Gottingen: Gottingen, Germany, 1997.

[36] K. Brandenburg, DIAMOND Version 3.2, Crystal Impact GbR: Bonn,Germany. 2007-2012.

[37] S. K. Wolff, D. J. Grimwood, J. J. McKinnon, M. J. Turner, D. Jayatilaka, M. A. Spackman, CrystalExplorer 3.1,University of Western Australia, 2012.

[38] M.A. Spackman, D. Jayatilaka, Hirshfeld surface analysis, CrysEngComm 11 (2009) 19-32. https://doi.org/10.1039/B818330A .

[39] R. Ayadi, J. Lhoste, I. LedouxRak, T. Mhiri, M. Boujelbene, Crystal structure, Hirshfeld surface analysis, thermal behavior and IR investigation of a new organic selenate-selenide $[C_3H_{12}N_2]_2(SeO_4)(SeO_3)\cdot{}_4H_2O$, J. Saudi Chem. Soc.21 (7) (2017) 869-877. https://doi.org/10.1016/j.jscs.2017.05.001 .

[40] J.J. McKinnon, D. Jayatilaka, M.A. Spackman, Towards quantitative analysis of intermolecular interactions with Hirshfeld surfaces, Chem. Commun. 37 (2007) 3814. https://doi.org/10.1039/B704980C .

[41] M.A. Spackman, P.G. Byrom, A novel definition of a molecule in a crystal J. Phys. Lett. 267 (1997) 215–220. https://doi.org/10.1016/S0009-2614(97)00100-0 .

[42] M J. Frisch, G W. Trucks, H.B. Schlegel, G.E. Scuseria, M.A. Robb, J.R. Cheeseman, G. Scalmani, V. Barone, B. Mennucci, G.A. Petersson, H. Nakatsuji, M. Caricato, X. Li, H.P. Hratchian, A.F. Izmaylov, J. Bloino, G. Zheng, J.L. Sonnenberg, M. Hada, M. Ehara, K. Toyota, R. Fukuda, J. Hasegawa, M. Ishida, T. Nakajima, Y. Honda, O. Kitao, H. Nakai, T. Vreven, J.A. Montgomery, J.E. Peralta, F. Ogliaro, M. Bearpark, J.J. Heyd, E. Brothers, K.N. Kudin, V.N. Staroverov, R. Kobayashi, J. Normand, K. Raghavachari, A. Rendell, J.C. Burant, S.S. Iyengar, J. Tomasi, M. Cossi, N. Rega, J.M. Millam, M. Klene, J.E. Knox, J.B. Cross, V. Bakken, C. Adamo, J. Jaramillo, R. Gomperts, R.E. Stratmann, O. Yazyev, A.J. Austin, R. Cammi, C. Pomelli, J.W. Ochterski, R.L. Martin, K. Morokuma, V.G. Zakrzewski, G.A. Voth, P. Salvador, J.J. Dannenberg, S. Dapprich, A.D. Daniels, €O. Farkas, J.B. Foresman, J.V. Ortiz, J. Cioslowski, D.J. Fox, GAUSSIAN 09, Revision A.1, GAUSSIAN, Inc, Wallingford CT, 2009. https://gaussian.com/g09citation/ .

[43]A D. Becke, Density-functional thermochemistry. IV. A new dynamical correlation functional and implications for exact-exchange mixing, J. Chem. Phys. 104 (1996) 1040. https://doi.org/10.1063/1.470829 .

[44] C. Lee, W.W. Yang, R.G. Parr, Development of the Colle-Salvetti correlation-energy formula into a functional of the electron density, Phys. Rev. B 37 (1988) 785. https://doi.org/10.1103/PhysRevB.37.785 .

[45] R.G Parr, W Wang, DensityeFunctional Theory of Atoms and Molecules,Oxford University Press, New York (1989).

[46] S. Chiodo, N. Russo, E. Sicilia, LANL2DZ basis sets recontracted in the framework of density functional theory, J. Chem. Phys. 125 (2006) 104. https://doi.org/10.1063/1.2345197 .

[47] H B. Schlegel, Optimization of equilibrium geometries and transition structures, J. Comput. Chem. 3 (1982) 214-218. https://doi.org/10.1002/jcc.540030212 .

[48] National Institute of Standards and Technology (NIST), Computational Chemistry Comparison and Benchmark Database: Precomputed Vibrational Scaling Factors. http://cccbdb.nist.gov/vibscalejust.asp.

[49] K. Holderna-Natkaniec, M.O.M. Sghaier, P. Ławniczak, M. Zdanowska Fraczek, A. Wozniak-Braszak, S. Chaabouni, Electric properties and internal dynamics of the $[C_6H_{18}N_2]$ $SbCl_5$ $[C_6H_{18}N_2]$ Cl_2 in intermediate temperature phase (part II), Polyhedron 85 (2015) 131–136 . https://doi.org/10.1016/j.poly.2014.08.044 .

[50] L. Pauling, The nature of chemical bond; Itca: Cornell Univ.Press, 260 (1960).

[51] H. Terao, S. Ninomiya, M. Hashimoto, K. Eda, ^{81}Br NQR and crystal structure of 4-bromopyridinium pentabromoantimonate(III); 3c–4e bonding and NQR trans influence ,J. Mol. Struc. 965 (2010) 68-73. https://doi.org/10.1016/j.molstruc.2009.11.040 .

[52] C.-Y. Mao, W.-Q. Liao, Z.-X. Wang, Z. Zafar, P.-F. Li, X.-H. Lv, D.-W. Fu, Temperature-Triggered Dielectric-Optical Duple Switch Based on an Organic-Inorganic Hybrid Phase Transition Crystal: $[C_5N_2H_{16}]_2SbBr_5$, Inorg. Chem. 55 (2016) 7661. https://doi.org/10.1021/acs.inorgchem.6b01107 .

[53] M. Ben Taher, N. Chaari, M. Ben Bechir, S. Chaabouni1, X-ray diffraction, vibrational properties, and dielectric studies of 3-ammoniumpropyl imidazolium pentabromoantimonate (III), J.Appl. Phys. A 123 (2017) 285. https://doi.org/10.1007/s00339-017-0895-4 .

[54] S. Chaabouni, S. Kamoun, J. Jaud, Crystal structure of $NH_3(CH_2)_2NH_3BiCl_5$-$2H_2O$, J. Chem. Crystallogr. 28 (1998)209. https://doi.org/10.1023/A:1022474327917 .

[55] J. Zaleski, A. Pietraszko, Structure at 200 and 298 K and X-ray investigations of the phase transition at 242 K of $[NH_2(CH_3)_2]_3Sb_2Cl_9$ (DMACA). Acta Crystallogr. B 52/2, 287 (1996). https://doi.org/10.1107/S0108768195010615 .

[56] Addison, A. W.; Rao, N. T.; Reedijk, J.; van Rijn, J.; Verschoor, G. C. (1984). "Synthesis, structure, and spectroscopic properties of copper(II) compounds containing nitrogen–sulphur donor ligands; the crystal and molecular structure of aqua[1,7-bis(N-methylbenzimidazol-2′-yl)-2,6-dithiaheptane]copper(II) perchlorate". J. Chem. Soc., Dalton Trans.: 1349. doi:10.1039/dt9840001349.

[57] M.O.M. Sghaier, K.H. Natkanec, A.W. Braszak, P. Czarnecki, S. Chaabouni, Structure and internal dynamics of N,N-diethylethylendiammonium pentachloroantimoniate(III)–N,N-diethylethylendiammonium dichloride, Polyhedron 70 (2014) 85–91. https://doi.org/10.1016/j.poly.2013.12.011 .

[58] Z. Aloui, V. Ferretti, S. Abid, M. Rzaigui, C. Ben Nasr, Synthesis, crystal structure and characterization of two new organic bismuthate(III) compounds: $[C_6H_{18}O]_2Bi_2X_{10}2H_2O$ (X= Br, Cl), J. Therm. Anal. Calorim. 121 (2015) 613-618. https://doi.org/10.1007/s10973-015-4634-9 .

[59] M. Essid, Z. Aloui, V. Ferretti, S. Abid, F. Lefebvre, M. Rzaigui, C. Ben Nasr, Crystal structure, Hirshfeld surface and spectroscopic studies of the noncentrosymmetric Bi(III) halide complex: $[C_8H_{12}N]_3BiCl_6$, Inorg. Chim. Acta. 457 (2017) 122-129. https://doi.org/10.1016/j.ica.2016.12.012 .

[60] Rahul Soman, Subramaniam Sujatha, Chellaiah Arunkumar, Quantitative crystal structure analysis of fluorinated porphyrins , Journal of Fluorine Chemistry 163 (2014) 16–22. https://doi.org/10.1016/j.jfluchem.2014.04.002 .

[61] R .Dennington, T. Keith, J. Millam, GaussView, Version 5, Semichem Inc, Shawnee Mission, KS, 2009.

[62] T. Guerfel, A. Gharbi, A. Jouini, crystal structure, thermal analysis and ir investigation of n,n,n',n'-tetra methyl ethylene diammonium sulfate dehydrate, J. Soc. Alger. Chim. 17 (2007) 125. https://www.researchgate.net/publication/272418256 .

[63] F. Şen, S. Kansiz and İ. Uçar , A one-dimensional copper(II) coordination polymer incorporating succinate and N , N -diethylethylenediamine ligands: crystallographic analysis, vibrational and surface features, and DFT analysis, Acta Cryst. (2017) 517-524 . https://doi.org/10.1107/S2053229617008452.

[64] M.A. Ben Abdallah, A. Bacchi, A. Parisinid, P.P. Mazzeo, F. Terenziani, L. Marchiò and S. Kamoun, Structure, vibrational, electrical and optical study of $[C_2H_{10}N_2]$ $(IO_3)_2 \cdot 4HIO_3$, J. Mol. Struct.1179 (2018) 18-32 . https://doi.org/10.1016/j.molstruc.2018.10.098 .

[65] B. V. Bukvetskii, T. V. Sedakova, A. G. Mirochnik, Crystal Structure And Luminescence Of Antimony(Iii) Bromide With Aniline, Struct. Chem. 50 (2) (2009) 322-327. https://doi.org/10.1007/s10947-009-0044-9 .

[66] M.S. Lassoued, M.S.M. Abdelbaky, A. Lassoued, R. Mendoza Meroño, A. Gadri, S. Ammar, A. Ben Salah, S. Garcia Granda, . Synthesis, crystal structure, vibrational spectroscopy and photoluminescence of new hybrid compound containing chlorate anions of stanate (II) , J. Mol. Struct. 1141 (2017) 660-667. https://doi.org/10.1016/j.molstruc.2017.03.124 .

[67] H. Dammak, A. Yengui, S. Triki, Y. Abid, Structural characterization, vibrational, optical properties and DFT investigation of a new luminescent organic–inorganic material: $(C_6H_{14}N)_3Bi_2I_9$, J. Lumin. 161 (2015) 214-220. https://doi.org/10.1016/j.jlumin.2015.01.010 .

[68] H. Dammak, A.Yengui, S.Triki, Y.Abid, H.Feki, Structural, vibrational and optical properties of a new self assembled organic–inorganic nanowire crystal (C6H14N)2[BiBr5]. A Density Functional Theory approach J. Lumin. 166 (2015) 180-186. https://doi.org/10.1016/j.jlumin.2015.05.031 .

[69] Da Chen, Fulong Dai, Shiqiang Hao, Guojun Zhou, Quanlin Liu, Christopher Wolverton, Jing Zhao, and Zhiguo Xia , Crystal Structure and Luminescence Properties of Lead- Free Metal Halides: $(C_6H_5CH_2NH_3)_3MBr_6$ (M = Bi and Sb) . DOI: 10.1039/x0xx00000x .

[70] Zhifang Tan , Manchen Hu, Guangda Niu , Qingsong Hu, Jinghui Li, Meiying Leng, Liang Gao, Jiang Tang , Inorganic antimony halide hybrids with broad yellow emissions,j. Science Bulletin 64 (2019) 904–909 . https://doi.org/10.1016/j.scib.2019.05.016 .

[71] Fengxia Wei, Zeyu Deng, Shijing Sun, Noor Titan Putri Hartono, Hwee Leng Seng, Tonio Buonassisi, Paul . Bristowe, Anthony K. Cheethamb, Enhanced Visible Light Absorption for Lead-free Double Perovskite $Cs_2AgSbBr_6$,J. Communication (2012) 1-3 . DOI: 10.1039/x0xx00000x .

[72] George C. Anyfantis, Nikolaos-Minas Ganotopoulos, Aikaterini Savvidou, Catherine P. Raptopoulou, Vassilis Psycharis, George A. Mousdis, Synthesis and characterization of new organic–inorganic hybrid compounds based on Sb, with a perovskite like structure , Polyhedron (2018) .https://doi.org/10.1016/j.poly.2018.05.024 .

[73] K. Oldenburg, A. Vogler, I. Miko, O. Horvath, Photoredox decomposition of tin(II), lead(II), antimony(III) and bismuth(III) iodide complexes in solution, Inorg. Chim. Acta. 248 (1) (1996)107-110. https://doi.org/10.1016/0020-1693(95)04980-0 .

[74] A. Vogler, A. Paukner, H. Kunkely, Photochemistry of coordination compounds of the main group metals, Coord. Chem. Rev. 97 (1990) 285-297. https://doi.org/10.1016/0010-8545(90)80096-C .

[75] A. Vogler, H. Nikol, Photochemistry and photophysics of coordination compounds of the main group metals , J. Pure Appl. Chem. 64(1992) 1311-1317. https://doi.org/10.1351/pac199264091311 .

Figures

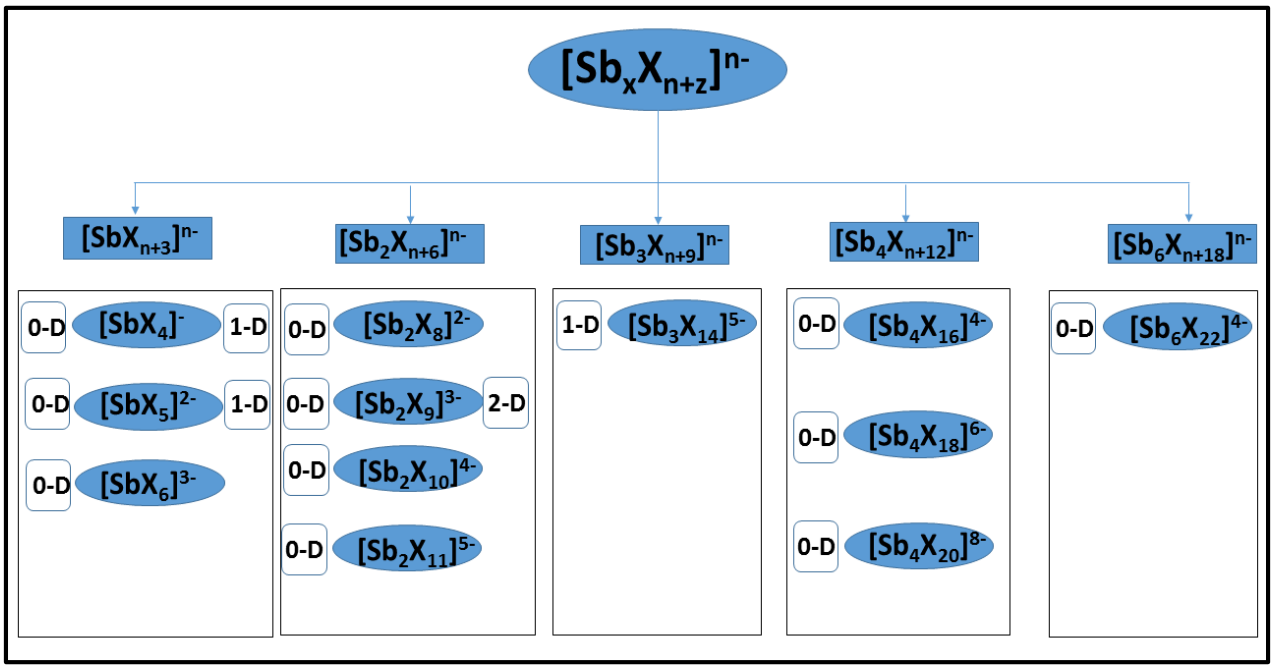

Fig.1: The different types of arrangement identified for the $[Sb_yX_{n+z}]^{n-}$ groups.

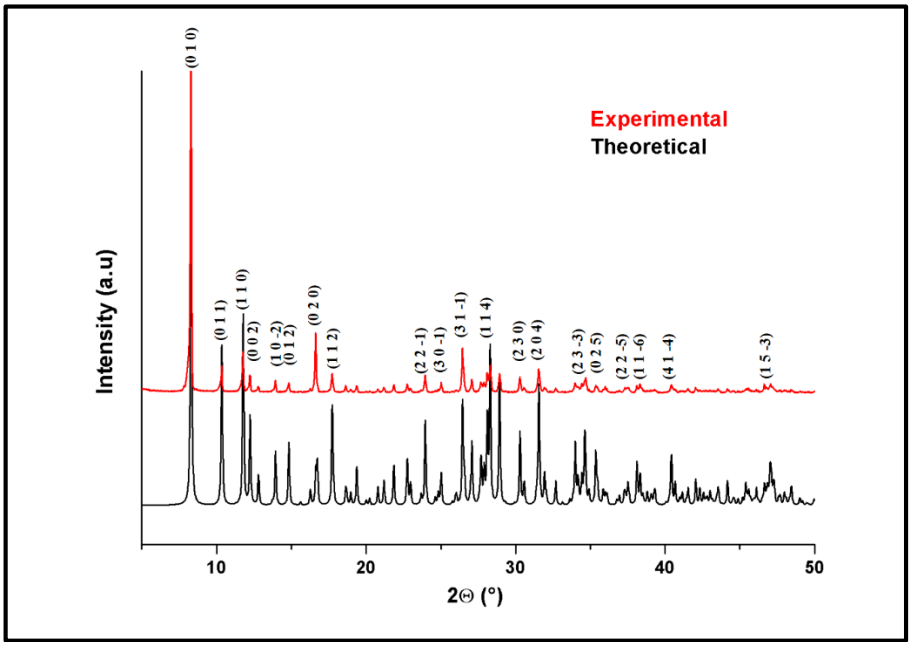

Fig.2: PXRD pattern of the compound compared with the calculated.

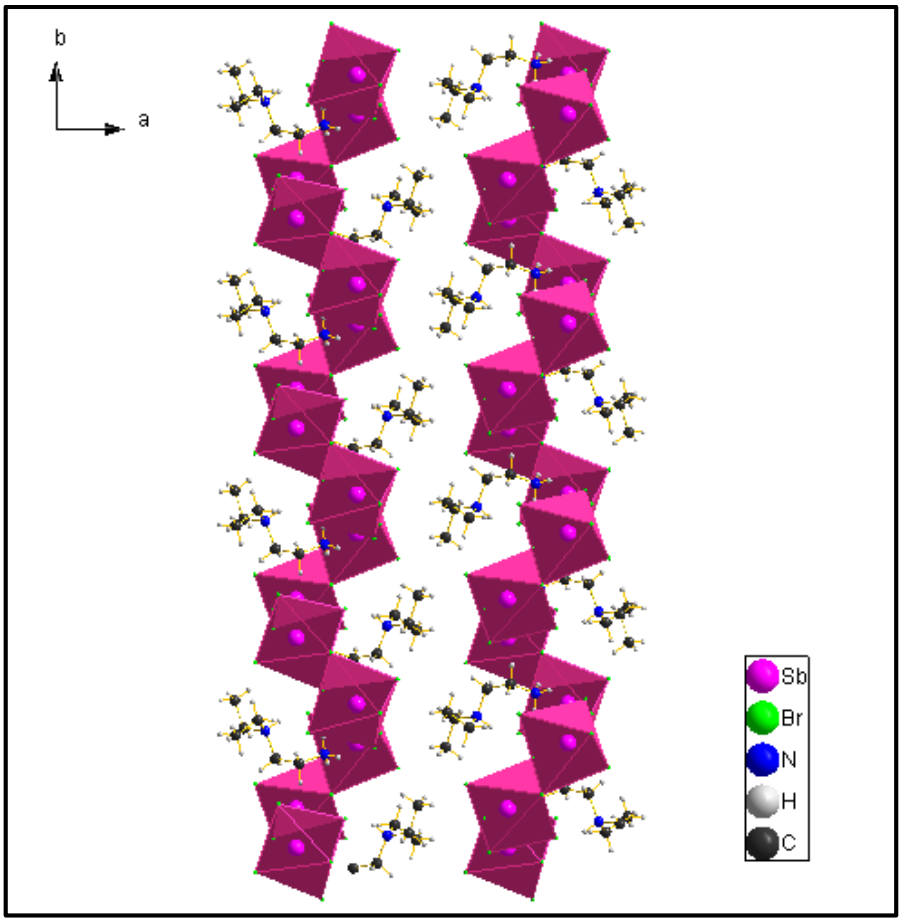

Fig.3: Projection of the structure in the ab plane. One-dimensional zig-zag $([SbBr_5]_n)^{2n-}$ chains along the b axis.

(a)

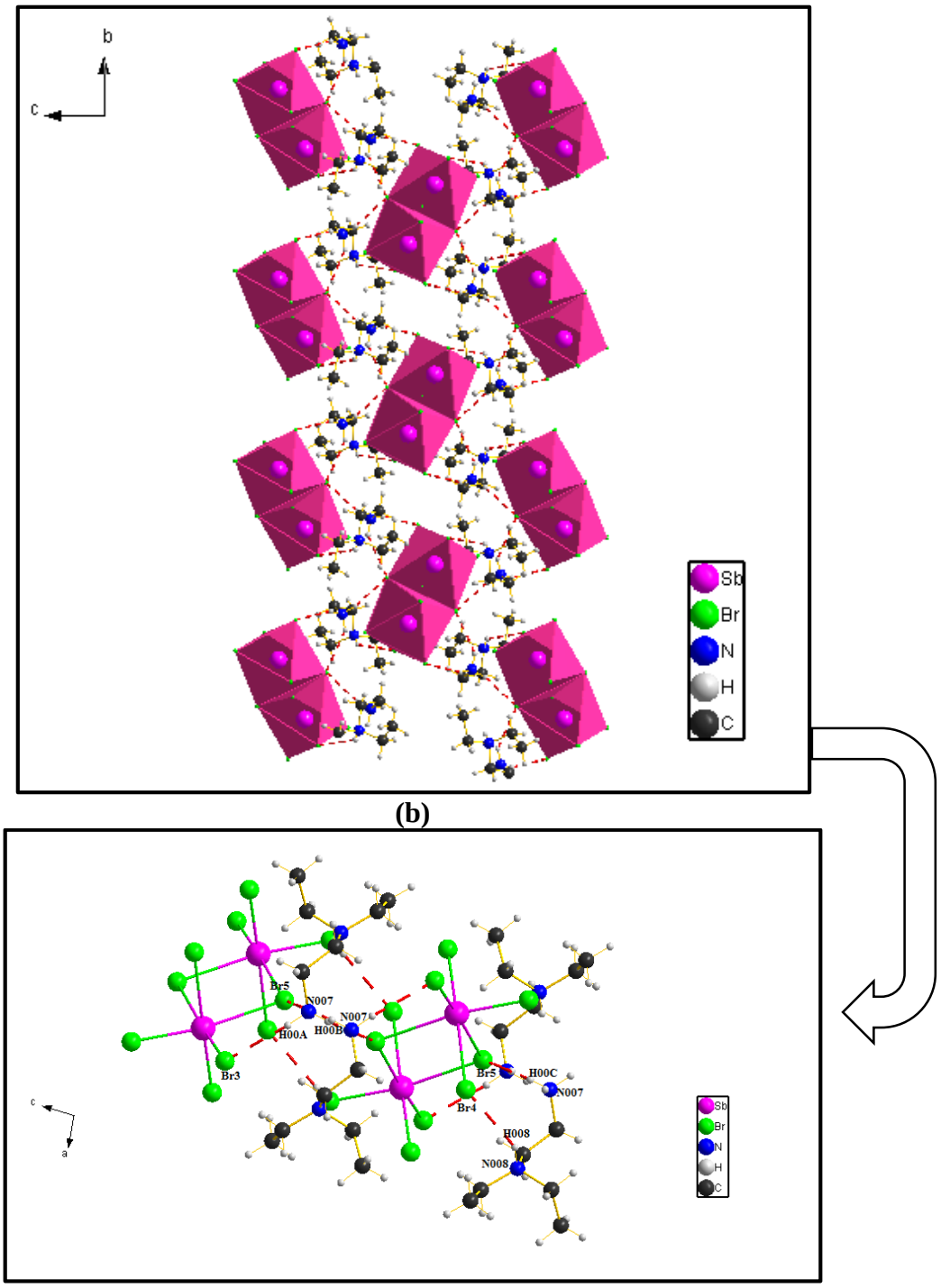

Fig.4: Projection of the structure in the (a) bc and (b) ac plane. N–H…Br hydrogen bonds.

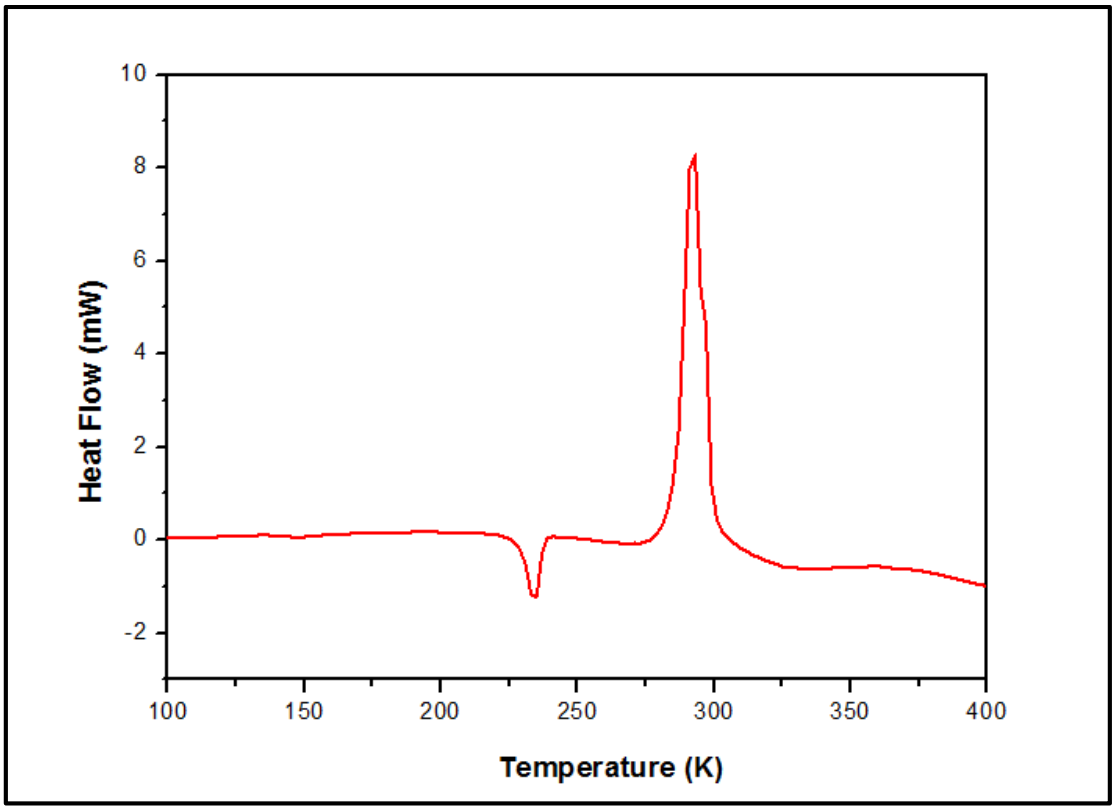

Fig.5: Calometric study of this compound.

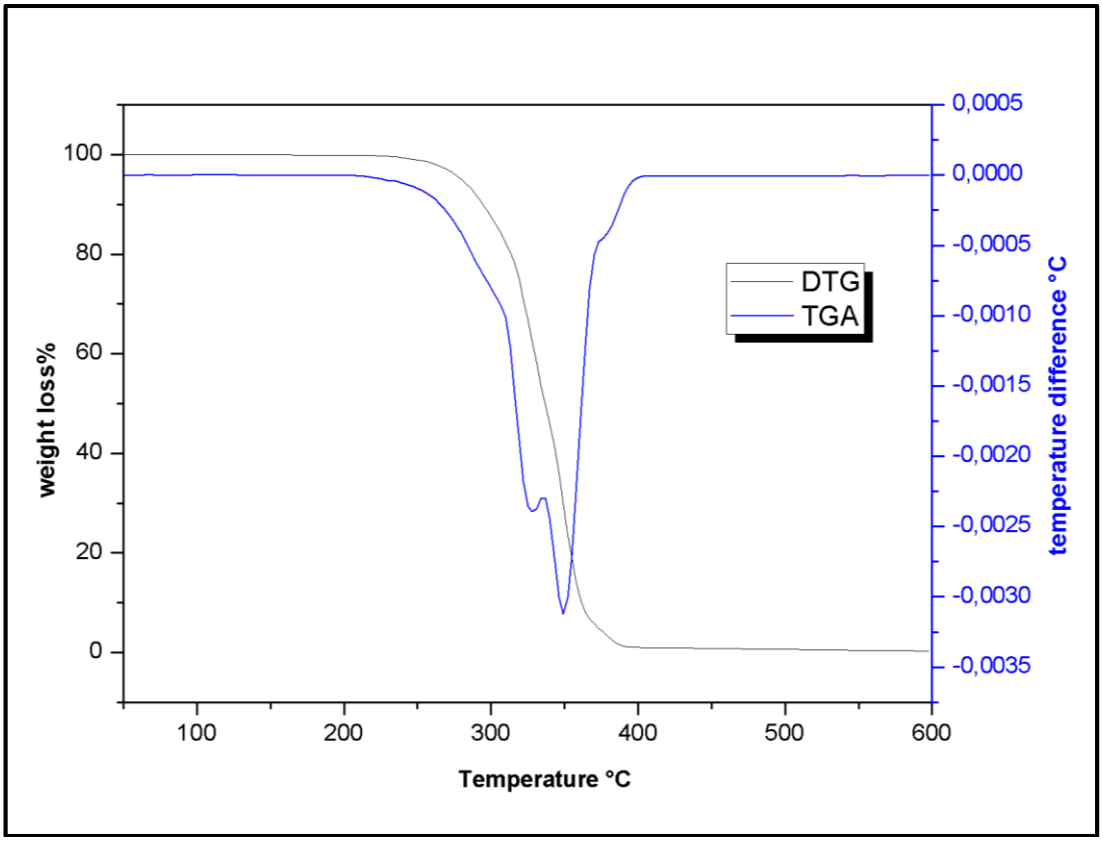

Fig.6: The TG/DTG curve of the compound in the 25-600°C range.

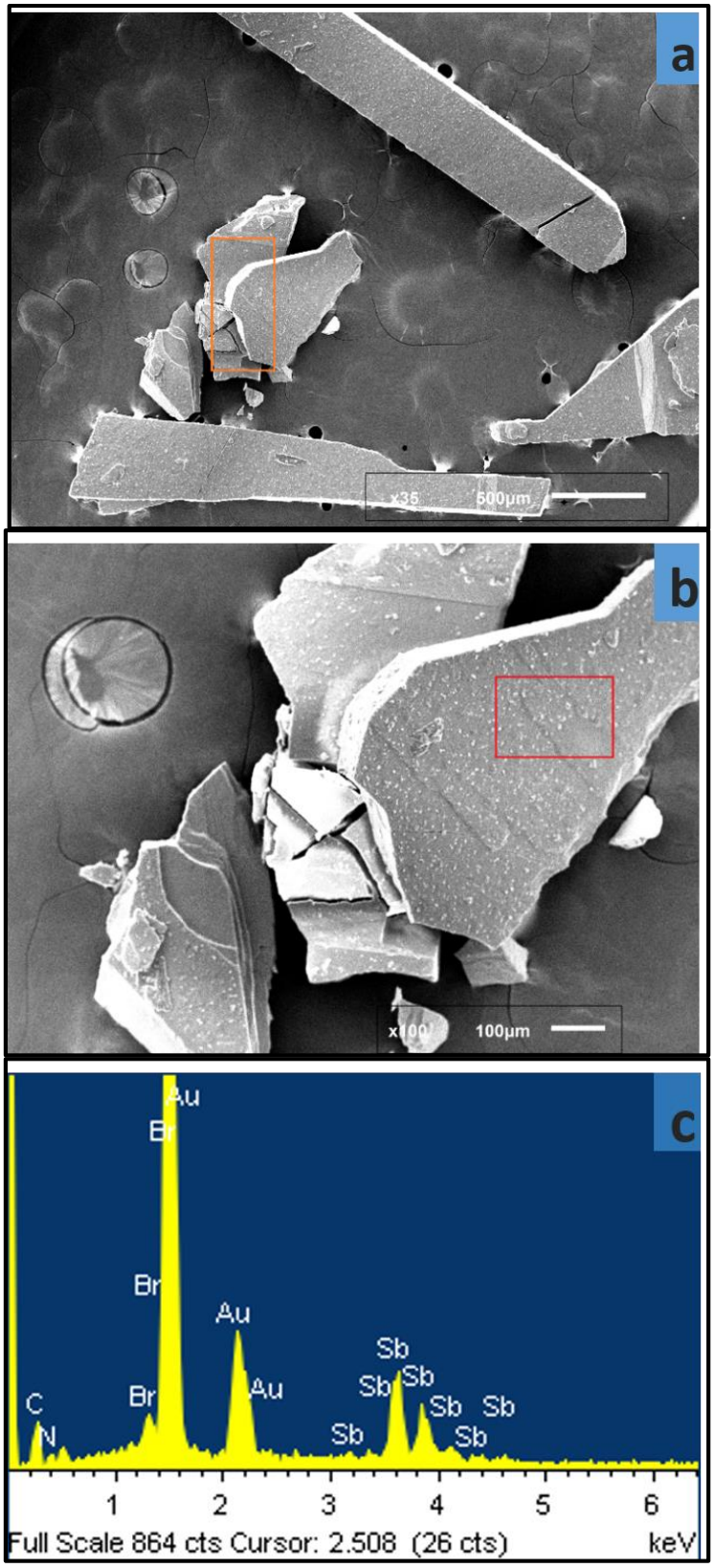

Fig.7: SEM images of the (a) surface morphology and (b) particle size and (c) typical EDX spectrum of $[C_6H_{18}N_2]_2Sb_2Br_{10}$.

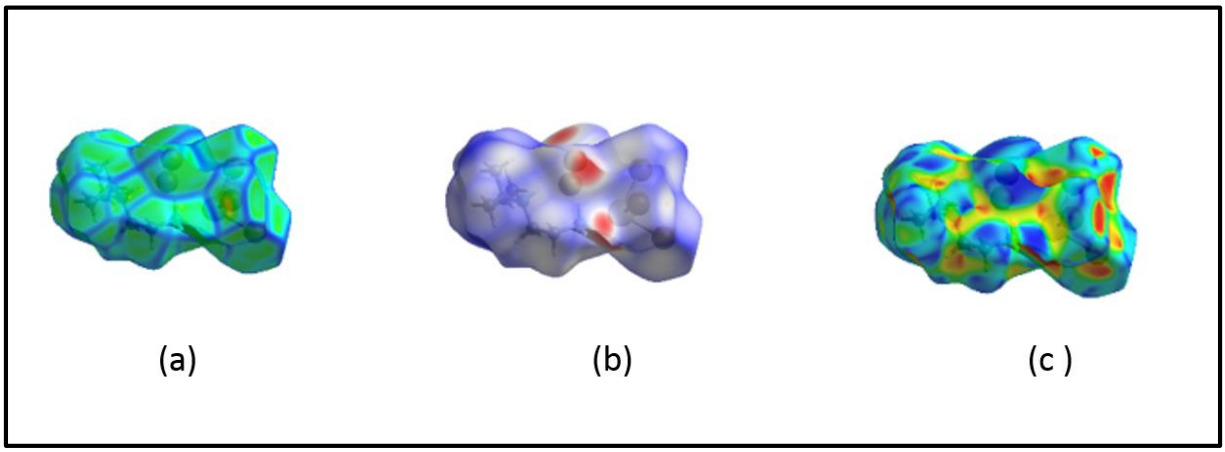

Fig.8: Hirshfeld surfaces mapped with *dnorm*(a), shape index (b) and curvedness (c) for the title compound.

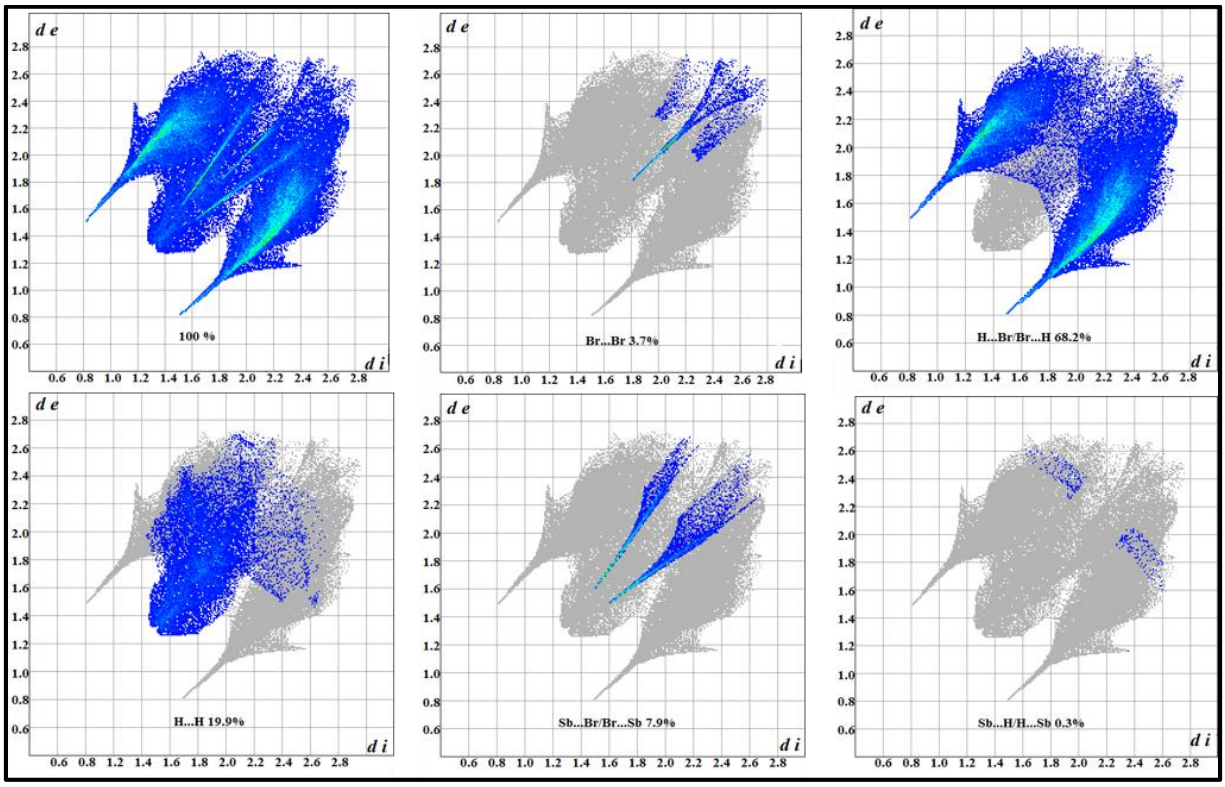

Fig.9: 2D fingerprint plots of the title compound.

(a)

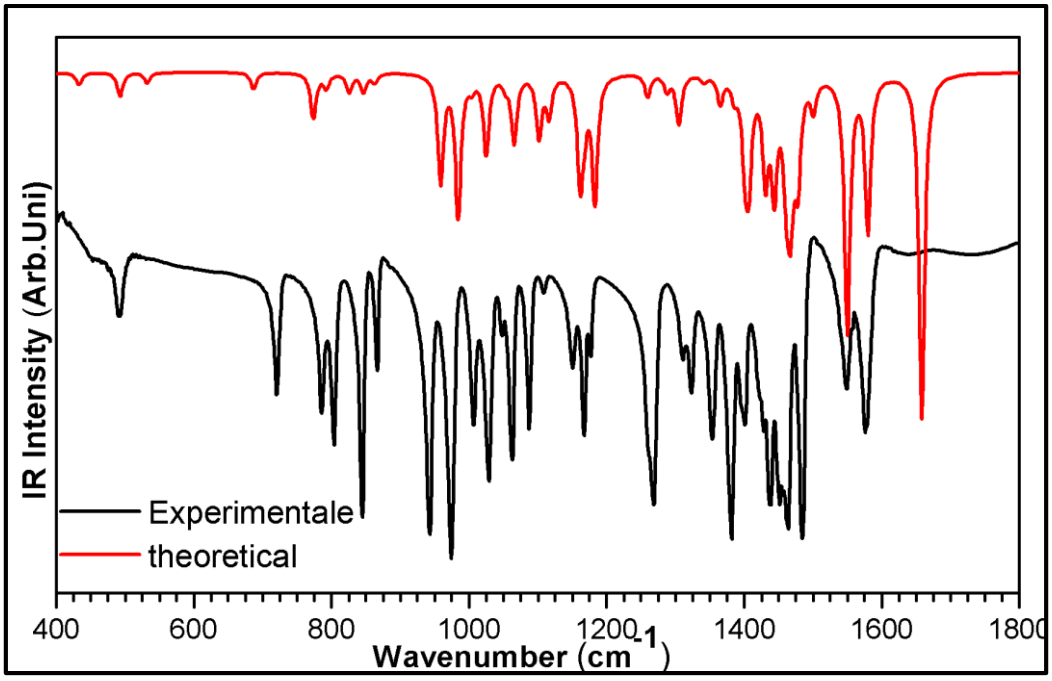

(b)

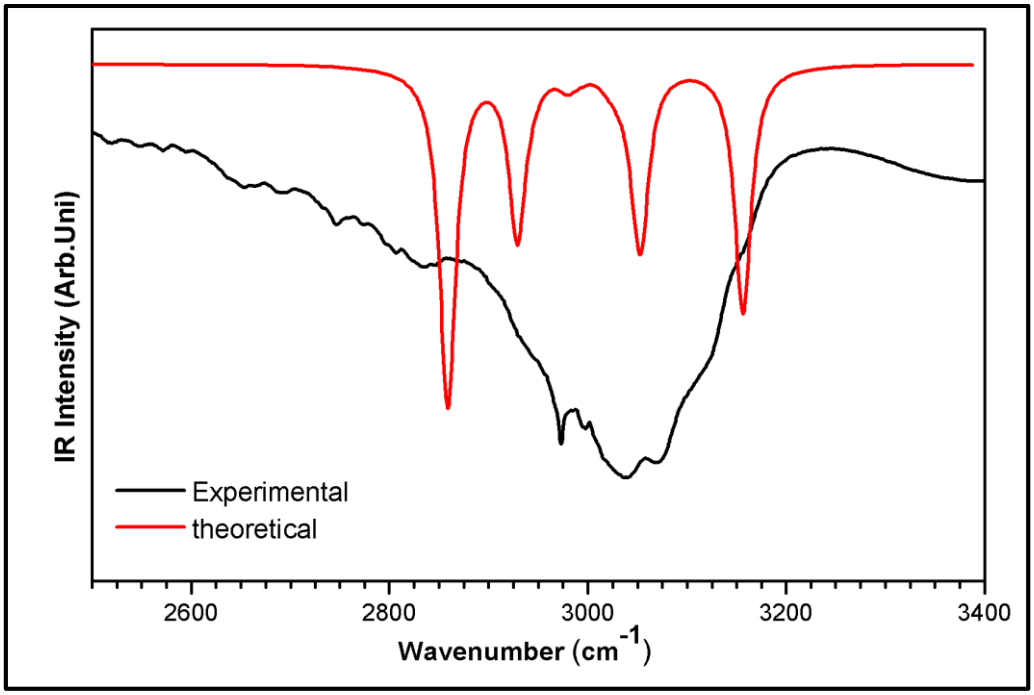

Fig.10: Experimental and theoretical IR absorption spectra of $[C_6H_{18}N_2]_2Sb_2Br_{10}$ in the (a) low and (b) high wavenumbers regions.

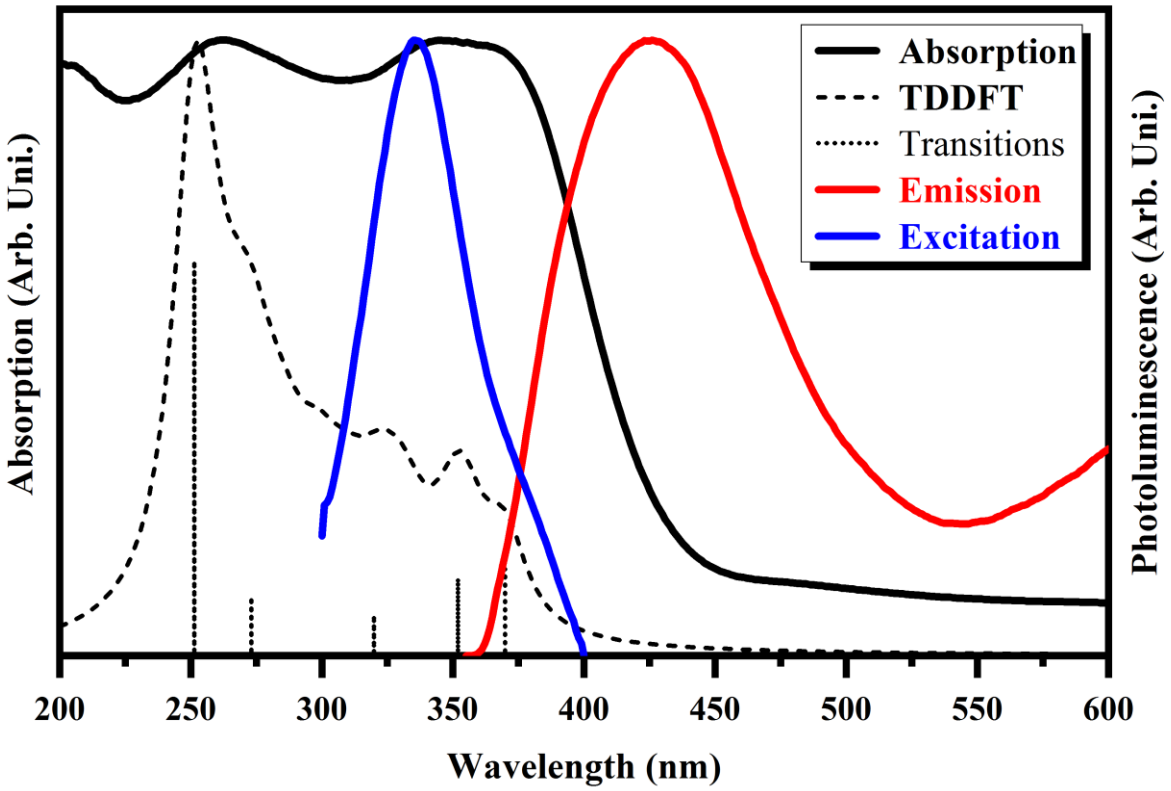

Fig.11: (Black) Experimental and theoretical UV-Visible absorption spectra, (red) emission and (blue) excitation spectra of $[C_6H_{18}N_2]_2Sb_2Br_{10}$.

Sheme1

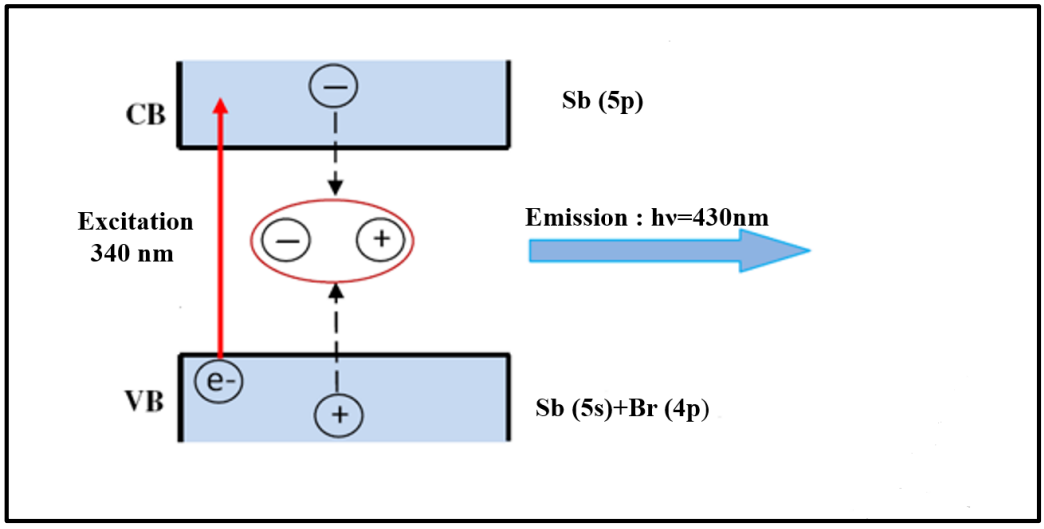

Table 1: Crystallographic data of $(C_6H_{18}N_2)_2\ Sb_2Br_{10}$

Crystal data	
Chemical formula	$(C_6H_{18}N_2)_2\ Sb_2Br_{10}$
Mr	1278.96
Crystal system, space group	Monoclinic, $P2_1/c$
Temperature (K)	293
***a, b, c* (Å)**	10.7309 (3) , 10.5842 (3), 14.5551 (4)
***β* (°)**	96.962 (3)
***V* (Å^3)**	1640.95 (8)
Z	4
Radiation type	Mo Kα (λ = 0.71073 Å)
μ (mm−1)	13.83
Crystal size (mm)	0.24 × 0.07 × 0.05
Data collection	
Diffractometer	Xcalibur, Ruby, Geminidiffractometer
Absorption correction	multi-scan
Tmin, Tmax	0.751, 0.804
No. of measured, independent and observed [I > 2σ(I)] reflections	23946 ,5076, 3362
R_{int}	0.082
hkl range	$h = -14 \rightarrow 15$ $k = -15 \rightarrow 13$ $l = -21 \rightarrow 21$
Refinement	
***R* [F^2> 2σ(F^2)], wR(F^2), S**	0.050 , 0.095 , 1.04
No. of reflections	5076
No. of parameters	117
Δρmax, Δρmin (e Å^{-3})	0.84 , −1.01
CCDC depositnumber	1842758

Table 2: Experimental and calculated bond lengths (Å) and angles (º).

Inorganic $[SbBr_6]^{2-}$octahedra			Organic $[C_6H_{18}N_2]^{2+}$ cation		
Bond	**Experimental**	**Theoretical**	**Bond**	**Experimental**	**Theoretical**
Sb1-Br1	2.6009 (7)	2.6705	C2-C1	1.503 (9)	1.533
Sb1-Br2	2.6128 (8)	2.8562	N008-C2	1.496 (7)	1.528
Sb1-Br3	2.6074 (7)	2.7770	N008-C3	1.502 (7)	1.539
Sb1-Br4	3.0681 (6)	3.1359	C3-C4	1.499 (9)	1.532
Sb1-Br5	3.2071 (8)	3.2176	N008-C5	1.499 (7)	1.533
Sb1-Br5i	3.2071 (8)	3.2187	C5-C6	1.493 (8)	1.531
Angle	**Experimental**	**Theoretical**	N007-C6	1.488 (8)	1.518
Br1-Sb1-Br2	92.81 (3)	96.69	**Angle**	**Experimental**	**Theoretical**
Br1-Sb1-Br3	89.29 (2)	91.52	C4-C3-N008	114.1 (5)	115.77
Br4-Sb1-Br1	187.84 (2)	166.54	C1-C2-N008	113.97(5)	113.96
Br5-Sb1-Br1	94.89 (3)	107.66	C6-C5-N008	116.2 (5)	117.62
Br3-Sb1-Br2	92.68 (2)	92.80	C2-N008-C5	110.2 (5)	108.22
Br4-Sb1-Br2	88.32 (2)	86.63	N007-C6-C5	113.1 (5)	113.73
Br2-Sb1-Br5	88.01 (2)	86.58	C5-N008-C3	113.3 (5)	114.18
Br3-Sb1-Br4	90.38 (4)	91.49	C2-N008-C3	113.9 (5)	115.23
Br3-Sb1-Br5	175.71 (2)	164.88			
Br4-Sb1-Br5	85.41 (2)	80.26			
Br3-Sb1-Br5i	93.78 (1)	102.02			
Br1-Sb1-Br5i	92.87 (2)	96.64			
Br2-Sb1-Br5i	171.43(3)	149.56			
Br5-Sb1-Br5i	85.13(3)	57.90			
Br4-Sb1-Br5i	86.02(2)	83.49			

Table 3: Distances Sb-Br (Å) of synthesized antimonite compounds.

Compound	**Sb-Br(Å)**	
	MIN	MAX
$[C_6H_{18}N_2]_2\ Sb_2Br_{10}$	2.67	3.22
$(C_4H_{12}N_2)_2[Sb_2Br_{10}]\cdot_2H_2O$	2.57	3.25
$(4\text{-}BrPyH)_2SbBr_5$ [51]	2.64	3.05
$4,40\text{-}C_{10}H_8N_2H_2)SbBr_5$	2.61	3.16
$(4\text{-}CH_3PyH)_2SbBr_5$	2.63	3.19

Table 4: Principal interatomic distances (Å) and bond angles (°) of the hydrogen bonding scheme.

D—H···A	**D—H**	**H···A**	**D···A**	**D—H···A**
N007—H00A···Br3$^{(i)}$	0.89	2.58	3.422 (4)	158
N007—H00B···Br5	0.89	2.60	3.374 (4)	145
N007—H00C···Br5$^{(ii)}$	0.89	2.42	3.291 (4)	167
N008—H00B···Br4$^{(iv)}$	0.91	2.69	3.424 (4)	139

Symmetry code ; (i) -x , 1-y ,-z; (ii) -x, 1/2+y, 1/2-z; (iii) -x, -1/2+y, 1/2+z

Table 5 : observed and calculated SEM and Elemental analyses of the compound .

Element	Experimental (%)	Theoretical(%)
antimony	2.61	2.53
Bromine	12.07	12.10
Carbon	61.78	61.75
Nitrogen	23.54	23.62

Table 6: Experimental and theoretical IR absorption wavenumbers (cm^{-1}) and corresponding assignments.

Experimental	Theoretical	Assignments
3157	3156	νa (NH3)
3125	-	νs (NH3)
3070	3052	νa (CH2)
3038	3030	νa (CH3)
2998	2979	νs (CH2)
2972	2940	νs (CH3)
2930	2928	ν (N-H…Br)
2836	2858	ν (NH)
1640	1658	δa (NH3)
1576	1579	
1549	1550	δs (NH3)
1506	1500	δ (CH2)
1484	1477	δa (CH3)
1463	1466	
1451	1443	δ (CH2)
1437	1431	δ (NH)
1429		
1401	1404	δs (CH3)
1382	1386	ω (CH2)
1354	1365	
1322	1341	
1311	1305	t (CH2)
1267	1288	
1262	1259	
1177	1182	ρ (NH3)
1167		
1150	1161	
1108	1115	ρ (CH3)
1088	1101	
1062	1065	ν (CN)
1049	1054	ν (CC)
1029	1024	ν (CN)

1006	1002	ν (CC)
974 943	984 958	ρ (CH2)
888	861	δ (CNC)
866 845	846 825	δ (CCN)
804	791	δ (CNC)
785	773	δ (CH2)
720	687	δ (CNC)
-	531	
491	492	
???	432	

Abbreviations:*ν*: stretching; νas: asym stretching; νs: sym stretching; *δ:* scissoring;ρ: rocking;ω: wagging; t:twisting.

Table 7: Observed absorption bands and computed electronic transitions from TDDFT calculation.

Experimental	**Theoretical**		
λ_{max} (nm)	**Transition (nm)**	**Oscillator strength**	**Attribution***
355	369.93	0.0582	HOMO → LUMO (91%)
	354.90	0.0338	HOMO → LUMO+1 (91%)
	319.86	0.0270	HOMO-1 → LUMO (83%)
262	273.06	0.0393	HOMO-2 → LUMO (84%)
	251.33	0.2642	HOMO-2 → LUMO+1 (80%)

* HOMO = High Occupied Molecular Orbital; LUMO = Low Occupied Molecular Orbital.